Effect of GPTMS functionalization on the improvement of the pH-sensitive Methyl red photostability

Maria Rosaria Plutino[a], Emanuela Guido[b], Claudio Colleoni[b], Giuseppe Rosace[b,*]

[a] Institute for the Study of Nanostructured Materials, ISMN – CNR, O.U. Palermo, c/o Department of Chibiofaram, University of Messina, Viale F. Stagno d'Alcontres 31, Vill. S. Agata, 98166 Messina, Italy

[b] Department of Engineering and Applied Sciences, University of Bergamo, Viale Marconi 5, 20244 Dalmine, Bg, Italy

Abstract

The photostability of silylated Methyl Red (MR-GPTMS) dyestuff at 360 nm and under Visible light was investigated in water solution, in comparison to that of pure Methyl Red (MR). Both the dyestuffs were found relatively stable under visible light, while substantial decomposition, with different reaction times, occurs under UV irradiation, also on dependence of the pH value. In order to elucidate the mechanism of the color fading, a detailed spectroscopic study of the chemical structure of both molecules (i.e. MR and MR-GPTMS) was performed by means of UV-Vis, IR and NMR techniques, together with the employment of semi-empirical calculations. In the case of the functionalized MR-GPTMS dyestuff, an interesting behavior was found at acidic pH in comparison to the free MR: the presence of the bound GPTMS produces a decrease of the dyestuff decomposition rate of one order of magnitude. As a matter of fact, the functionalized azo-dye retains its pH-sensing behavior, while it improved significantly the sol-gel functionalized MR-GPTMS dye photostability. The rates of decolorization were found to fit a pseudo-first-order kinetic model. The enhanced stability is due to the covalent bond between the carboxyl group of azo dye

and the opened epoxy group of GPTMS. This functionalization increase the polarity of silylated Methyl Red in the region of the azo group and consequently the surrounding electron density making it less susceptible to cleavage by hydroxyl radicals attack.

The analysis of the photolyzed products using Fourier Transform Infrared Spectroscopy (FTIR) further confirms that the ultraviolet degradation of both dyestuffs proceeded by following the same reaction pathway.

Keywords: Sol–gel; 3-glycidoxypropyltrimethoxysilane; Methyl Red; Hydrogen bonding; pH-sensor.

1. Introduction

The development of novel treatments of textile fabric surfaces has attracted considerable attention across many scientific disciplines with interesting ranging from fundamental research to practical applications [1]. In recent years, Hybrid Organic-Inorganic Materials (HOIM) have fascinated the scientific community for fundamental research and technological applications thanks to their novel and well-defined structure together with their unique optoelectronic properties. In particular, the incorporation of organic and biological molecules into nano-porous silica sol–gel hosts can open new research perspectives. Aside from being biocompatible, the porous inorganic silica matrix has demonstrated to enhance the thermal stability of coated polymers [2] and the thermodynamic stability of encapsulated guest molecules, mostly credited to the effect of cage confinement on molecular motions. Thus, it is well-known that organic dyes gain an exceptional photostability when entrapped inside silica sol–gel matrixes [3]. Since the beginning in 1984, [4] the sol–gel method has allowed the encapsulation of many types of molecules in oxide gels [5-8] and the optical properties of these systems have been studied [9,10]. This encapsulation is usually accomplished using either doping or grafting processes to give organo-functional sol–gel materials.

Doping technique, involving the physical entrapment of a reagent inside the substrate, is simple and applicable to many organic compounds, but the pore size must be carefully tailored, as dopant leaching is often a problem. On the other side, grafting technique, involving a reagent anchoring through covalent bonding, yield highly reproducible, stable products, but the overall process can be quite laborious. The silyl reagents need to contain a $–Si(OR)_3$ group, and this condition limits the selection of reagents suitable for the grafting processes. The porous nature of sol–gels allows for the delivery of analytes to the encapsulated reagent, resulting in the interactions required for sensing applications.

Recently, HOIM obtained by sol–gel methodologies find manifold interest in textile field, where they are regularly used to induce hydrophobicity [11], flame retardant [12,13], antimicrobial [14,15], self-cleaning [16] properties or to immobilize dyestuffs on textile fabrics [17]. These findings are particularly challenging to design innovative applications that exploit sol-gel methods also to development of textile materials with sensing properties [18,19].

The list of molecules that can be incorporated into matrices, for optical or electro-optical applications, are almost unlimited and include halochromic dyes, biological or enzymatic functional molecules and liquid crystals [20,21]. However, the physical entrapment of indicators in thin films does not make sensors usable over a period of several days or weeks [22]. In order to obtain stable sensors it is required to form more stable covalent [23] or electrostatical [24] binding of indicators to the solid matrix employed.

In the present work, the combination of the sol–gel process and the covalent binding for the immobilization of indicators was investigated with respect to the enhanced stability of the immobilized dyestuff. With this aim, leaching of the dye, which is a common phenomenon in traditional dyeing, may be minimized by applying a coupling agent giving a covalent bond between the silica sol and the pH-indicator molecule. In this way, the feasibility of introducing halochromic molecules into a sol–gel matrix obtained by 3-glycidoxypropyltrimethoxysilane (GPTMS), and the durability of the color change, also after immobilization onto textile fabrics, have been recently

demonstrated in our previous researches [19,25], monitoring changes in absorbance intensity associated with the protonation/deprotonation process on dedicated, compact solid-state instrumentation. Therefore, in this paper the sol–gel based functionalized Methyl Red (MR-GPTMS) was prepared and its photostability in aqueous solution was studied and compared to the free Methyl Red (MR) dyestuff. The MR, i.e. 2-(4-dimethylaminophenylazo)benzoic acid, a well-known non-polar mono azo dye, used as pH-indicator in the pH-region 4.4–6.0, was selected as pH-sensitive dye. MR is also used as coloring agents, acid-base indicators implementing proton-transfer reactions, and electrochemical species exercising electron-transfer reactions etc. [26]. Moreover, it is used as a dye for coloring textiles (cotton, wool, silks, and acrylics), china clay products, leather, printing inks, and as a filter dye in photography. Considering that, since to the best of our knowledge, no studies on this functionalized dyestuff have been reported so far, we decided to investigate the stability of this complex under UV as well as visible sources irradiation. The aim of the present study was to assess the photostability of both azo dye systems, MR and MR-GPTMS, including the examination of the relationship between the dye structure and photolysis, taking into special consideration the role of substitute in diazo component in ortho positions to the azo bond. The comparison between the dyestuff molecules was based on spectroscopic measurements, both for the color assessment and the degradation rates of dyestuffs.

2. Experimental

2.1. Materials and methods

Methyl Red (MR), GPTMS, Na_2HPO_4/citric acid buffers (A.R. grade) and other chemicals were purchased from Aldrich and used as received. By following our already reported procedure, [18] the functionalized dyestuff was synthesized by adding to an alcohol solution of GPTMS, MR (0.1:1 molar ratio with respect to GPTMS) in the presence of a catalytic amount of HCl (GPTMS:HCl:EtOH molar ratio of 1:0.008:60) and leaving the reaction mixture under stirring for 6

h at 70 °C. After this time, water was added to the mixture (GPTMS:H_2O molar ratio of 1:55) and the reaction was left to react further at 70 °C for 3 h. During this second step the hydrolysis and condensation reactions take place leading to a transparent orange hybrid sol (MR-GPTMS sol).

The influence of pH on the dyestuffs photostability was evaluated by using two different pH values, obtained by McIlvaine Na_2HPO_4/citric acid buffers [27]. Additions of buffer were minimized to avoid changing the volume of the reaction mixture.

2.2. Spectroscopic Characterization

All solutions were fully characterized by UV–Vis spectroscopy, in buffered solutions at different pH values, and by FTIR spectroscopy on solid residue. The Ultraviolet–Visible absorption spectra were recorded on a Thermo Nicolet Evolution UV–vis-500 spectrophotometer, using matched quartz cuvettes of 1 cm path length (Hellma, Germany). All spectra were recorded at room temperature from 250 to 800 nm. FTIR spectra were recorded with a Thermo Avatar 370, equipped with attenuated total reflection (ATR) accessory. A diamond crystal was used as internal reflectance element on the ATR accessory. Spectra were acquired, at room temperature, in the range from 4000 to 550 cm^{-1}, with 32 scans and a resolution of 4 cm^{-1}. The photostability of dye systems was assessed by monitoring dyestuff degradation after exposure of the solutions to UV (λ_{max} = 365 nm) or visible (day light lamp) sources. Irradiations were performed in a Helios Italquartz photochemical reactor equipped with 10 lamps. All NMR experiments were carried out in acetone-d_6 at 298.2 (± 0.1) K. The ^1H and $^{13}C\{1H\}$ NMR spectra were recorded on a Varian 500 spectrometer, equipped with a 5 mm OneNMR (TM) probe operating at 500.1 and 125.7 MHz. All chemical shifts are reported in parts per million (δ / ppm), downfield to tetramethylsilane (Me_4Si) as an internal standard (δ = 0.0 ppm), or referenced to the residual protiated solvent signal such as in acetone-d_6 (^1H NMR: 2.05 ppm and ^{13}C NMR: 29.9 and 206.7 ppm); coupling constants *J* are given in Hertz. The purity of all starting materials as well as the reaction products characterization were determined by ^1H NMR assignment. ^1H and $^{13}C\{1H\}$ NMR resonances were assigned by means of

bidimensional homo- and heteronuclear NMR gradient experiments (gCOSY, ROESY, gHSQC and gHMBC). Gradient selected COSY, and ^{1}H-^{13}C Heteronuclear single and multiple bond correlations (HSQC and HMBC, respectively) spectra were acquired using the standard sequences as supplied by the VNMR software package. Two-dimensional Rotating frame nuclear Overhauser Effect Spectroscopy (ROESY) experiments were performed by employing a standard pulse sequence with a typical mixing time of 200 ms.

The water/ethanol content of the MR-GPTMS sol solution was kindly evaporated in a rotavapor apparatus for NMR characterization purpose.

4-Dimethylaminoazobenzene-2′-carboxylic acid (MR). ^{1}H NMR (500 MHz, acetone-d_6, 298 K) δ: 8.23 (d, $^{3}J_{HH}$ = 7.9 Hz, 1H, $H_{3'}$), 7.99 (d, $^{3}J_{HH}$ = 7.9 Hz, 1H, $H_{6'}$), 7.82 (d, $^{3}J_{HH}$ = 9.2 Hz, 2H, $H_{2,6}$), 7.72 (dd, $^{3}J_{HH}$ = 7.9 Hz, 1H, $H_{5'}$), 7.59 (dd, $^{3}J_{HH}$ = 7.9 Hz, 1H, $H_{4'}$), 6.96 (d, $^{3}J_{HH}$ = 9.2 Hz, 2H, $H_{3,5}$), 3.22 (s, 6H, N-CH_3).

^{13}C NMR (126 MHz, acetone-d_6, 298 K) δ: 166.0 (1C,*C*OOH), 154.5 (1C, C_1), 150.6 (1C, $C_{2'}$), 142.1 (1C, C_4), 133.4 (1C, $C_{5'}$), 131.9 (1C, $C_{3'}$), 129.7 (1C, $C_{4'}$), 126.6 (2C, $C_{2,6}$), 125.7 (1C, $C_{1'}$), 115.6 (1C, $C_{6'}$), 112.1 (2C, $C_{3,5}$), 39.5 (2C, N-*C*H$_3$).

4-Dimethylaminoazobenzene-2′-carboxylic acid, GPTMS ester (MR-GPTMS). ^{1}H NMR (500 MHz, acetone-d_6, 298 K) δ: 7.83 (d, $^{3}J_{HH}$ = 9.1, 2H, $H_{2,6}$), 7.54 (dd, $^{3}J_{HH}$ = 5.7 Hz, $^{4}J_{HH}$ = 3.5 Hz, 1H, $H_{6'}$), 7.51 (dd, $^{3}J_{HH}$ = 5.7 Hz, $^{4}J_{HH}$ = 3.5 Hz, 1H, $H_{3'}$), 7.29 (AB system, $^{3}J_{HH}$ = 5.7 Hz, $^{4}J_{HH}$ = 3.5 Hz, 1H, $H_{4',5'}$), 6.74 (dd, $^{3}J_{HH}$ = 9.1, 2H, $H_{3,5}$), 4.04 (m, br, $H_{5''}$, 1H), 3.70 (m, br, $H_{6''}$, 2H), 3.54 (m, br, buried under other signals, $H_{4''}$, 2H), 3.47 (m, br, buried under other signals, $H_{3''}$, 2H), 3.02 (s, 6H, N-CH_3), 1.67 (m, br, $H_{2''}$, 2H), 0.68 (m, br, $H_{1''}$, 2H).

^{13}C NMR (125.7 MHz, acetone-d_6, 298 K) δ: 175.3 (1C,*C*OOH), 152.5 (1C, C_1), 149.2 (1C, $C_{2'}$), 143.8 (1C, C_4), 140.7 (1C, $C_{1'}$), 128.7 (1C, $C_{5'}$), 127.6 (1C, $C_{4'}$), 127.5 (1C, $C_{3'}$), 125.1 (2C, $C_{2,6}$), 115.9 (1C, $C_{6'}$), 111.4 (2C, $C_{3,5}$), 71.5 (buried under other signals, 1C, $C_{4''}$), 66.4 (1C, $C_{3''}$), 63.3 (1C, $C_{6''}$), 61.0 (1C, $C_{5''}$), 39.6 (2C, N-*C*H$_3$), 22.8 (1C, $C_{2''}$), 7.8 (1C, $C_{1''}$).

Computational Details. Molecular mechanics MMFF94 force field and semi-empirical

calculations were performed on an Intel® core ™ i5 CPU personal computer (750 @2.67GHz and 8.00 GB RAM) using the Spartan package version '02. [28] The Methyl Red structure was properly modified and used as input for the calculations to gauge the performance of the MMFF94 calculations. Lowest-energy conformations of the neutral MR were generated by the systematic variation of the dihedral angles N-N-C1-C2. Full geometry optimization for each structure to a gradient convergence limit of less than 10^{-5} was carried out before a final single point energy calculation. During the minimization, no symmetry restriction was imposed. The six lowest energy structures were submitted to Spartan for PM3 semi-empirical calculations.

3. Results and discussion

3.1. UV-visible spectral characterization

3-glycidoxypropyltrimethoxysilane (GPTMS) precursor containing methoxysilyl groups and an epoxy group has been reacted with Methyl Red as reported in our previous study [18], with the aim to synthesize a novel pH-sensitive dye in order to develop a wearable textile-optoelectronic pH meter. The reaction scheme is shown in Scheme 1.

Scheme 1

The behavior in aqueous solutions of pure MR and sol-gel MR-GPTMS functionalized dyestuffs was investigated at different pH values, obtained with different buffered solutions. As expected, the position of the longest wavelength absorption band of azo dyes was sensitive to medium effects. Both MR and MR-GPTMS solutions visually changed color from yellow in alkaline or neutral solutions to red in acidic solutions.

Figure 1

To compare MR and MR-GPTMS water solutions, in Figure 1 the UV–visible spectra acquired in the range 250–800 nm at pH 2 and pH 8, after normalization of the spectra to a value of **1** at the peak maximum, are reported.

Both MR and MR-GPTMS change their color on protonation or de-protonation, while any change in their absorption peaks intensity occurs in dark until 10 h. Scheme 2 shows the equilibria taking place on MR dye upon acid/base addition in aqueous solution. It is clearly displayed that MR has a quinonoid form in acidic solution (HMR^+, red) and a benzenoid form in alkaline solution (MR^-, yellow), through a hydrazone-diazo tautomeric species conversion. Aqueous pure MR dye solution shows an absorption band which has an λ_{max} at 523 nm in acidic conditions (pH=2), responsible for the red color and ascribed to the HMR^+ cation (Scheme 2). Increasing the pH of solutions to 8, the absorption for acidic form disappears and moves at about 431 nm, giving a yellow final color, through orange step to the solution that may be attributed to the azo form of the anionic species MR^-. This is in accordance with Zhang et al. [29], who postulated that UV-visible electronic absorption spectra of methyl red aqueous solutions are characterized by the overlap of a principal peak at λ_{max} = 520±15 nm with a shoulder peak at λ_{max} = 435±20 nm, which are assigned to acidic species HMR^+ and basic species (MR^-) of methyl red, respectively.

Scheme 2.

Whereas the absorption bands in visible range are ascribed to the n→π* transition related to the chromophoric -N=N- group [30] of azo dyes, the bands in UV range are characteristics of the benzene ring of the dyes. Only one isosbestic point can be observed at 488 nm for MR dye, indicating that a two-composition equilibrium exists and varies with the acidity.

It is worthwhile to be noticed that the reaction with GPTMS has a marked influence on the color variation. While the color shifts of the MR solution turns from red (pH 2–4) to orange (pH 5)

and yellow (pH 6–8), the MR-GPTMS sol starts to be orange already at pH 4. The main difference is observed for the alkaline peak maximum (pH = 8) that shows a red shift from 431 nm in the pure MR solution to 456 nm in the MR-GPTMS diluted sol, due to the formed covalent bond between the carboxyl group of MR dye and the epoxy group of GPTMS in the derivative MR-GPTMS (as reported in Scheme 1). In the acidic conditions (pH = 2) the peak maximum do not substantially change (523 nm) because the MR fragment responsible for the color change is not altered by the covalent bond formation. Actually, in the new formed ester the halochromic spectroscopic change are essentially different from those observed for MR, since the carboxyl group is not anymore available to take part in the electronic delocalization of the different structural form of MR^- responsible for its characteristic color transitions. Since the electronic delocalization onto carboxylic group of MR is taking place under alkaline conditions, in the same pH conditions this is not anymore possible for MR-GPTMS due to the bond of the carboxyl moiety with the opened epoxy ring and the formation of an available acid hydroxyl group far away from it. The bathochromic shift of *ca* 25 nm, observed for MR-GPTMS sol at pH = 8, is an outcome of the inability to form zwitterionic and anionic derivatives of the MR molecule as shown in Scheme 2. These observations are in agreement with the literature data [31].

For this reason, the acid–base equilibrium of pure MR as reported in Eq. (1), can be expressed as in the reported Eq. (2) when the MR pH sensitive dye is bonded to GPTMS:

$$HMR^+ \underset{+H^+}{\overset{-H^+}{\rightleftharpoons}} MR \underset{+H^+}{\overset{-H^+}{\rightleftharpoons}} MR^- \qquad (1)$$

$$HMR^+\text{-GPTMS} \underset{+H^+}{\overset{-H^+}{\rightleftharpoons}} \text{MR-GPTMS} \qquad (2)$$

where HMR^+ and MR^- represent the protonated (acid) and the deprotonated (basic) forms of sensitive dye, while HMR^+-GPTMS and MR-GPTMS represent the corresponding protonated and the isoelectronic forms of the MR-GPTMS sol, respectively.

3.2. NMR characterization and structure determination

Proton and heteronuclear mono- and bi-dimensional NMR spectroscopy is a useful tool to: (i) ascertain the epoxy ring opening that from the starting GPTMS and the MR dye bring towards the formation of the sol derivative MR-GPTMS; (ii) assess the conformation of the nuclear species present in solution.

In the aliphatic region of the ^{1}H NMR spectrum of MR-GPTMS (upper side of Figure 2) it is evident a general shift of the proton signals belonging to the GPTMS fragment. The methinic $H_{5"}$ and the methylenic $H_{6"}$ protons are those mostly affected after the epoxy-ring opening reaction of GPTMS, showing a low-field shift after the ester bond formation with the MR dye. In particular the diastereotopic methylenic protons for $H_{6a,b}$ move from δ/ppm 2.77 and 2.57 chemical shifts in the free GPTMS, to a signal at 3.70 for $H_{6"}$ in MR-GPTMS. Moreover the methinic H_5 proton included in the epoxy ring changes from δ/ppm 3.11 to 4.04 relative to the C$H_{5"}$-OH proton formed after ring opening and hydrolysis reaction.

As a matter of fact the coalescence of the diastereotopic $H_{6a,b}$ protons in one broad singlet for $H_{6"}$ witnesses a release of the conformational oxirane ring strain towards the formation of the final ester product.

The occurred sol-gel reaction is also attested by: (i) the matching formation of free methanol at 3.28 ppm; (ii) the corresponding presence of Si-OH groups that give rise to a broad peak at 4.32 ppm in exchange with water and other OH groups (i.e. $CH_{5"}$-*OH*). Both these proton signals are due to hydrolysis/condensation reaction products of the GPTMS trimethoxysilane end, in agreement with already reported literature data [25,32].

In the aromatic region (lower side in figure 2) it is possible to notice the disappearance of the broad signal at 13.71 ppm relative to the acidic carboxylic proton. However the most relevant change is observed for the aromatic ring containing the carboxylic group in ortho position to the diazo bond. The $H_{3'}$ e $H_{6'}$ protons appear to be more shielded in the final MR-GPTMS derivative than those pertaining to the starting MR, thus resulting in a shift from the doublets observed at 8.23

and 7.99 ppm to a pair of closest doublets of doublets (*dd*) at 7.54 and 7.51 ppm in MR-GPTMS, respectively.

Additionally, the phenylic $H_{5'}$ and $H_{4'}$ protons (characterized in the starting MR by well-separated *dd* signals at δ/ppm 7.72 and 7.59, respectively) coalesce in an AB system lying at *ca* 7.29 ppm in MR-GPTMS. It is worthwhile to note that the marked shift at higher field of *ca* $\Delta\delta$ = 0.7 and 0.5 ppm for the two ortho $H_{3'}$ and $H_{6'}$ protons, respectively, is a further evidence of the formed ester bond between the MR dye and the silane fragment, by way of the epoxy-ring opening GPTMS reaction and covalent ester bond formation between the two starting moieties.

Figure 2

The highly deshielded position observed for the benzene $H_{3'}$ and $H_{6'}$ ortho-protons in the starting MR (i.e. higher chemical shift, δ =8.23 ppm and 7.99 ppm) is attributed to a combination of a strong polar effect and the diamagnetic anisotropy of the closest carbonyl and diazo groups. As also confirmed by the conformational structure obtained by semi-empirical calculations (right side of Figure 3), this experimental finding confirms that in the MR dye the carboxylic group itself lies in an almost locked six-ring conformation, due to the strong hydrogen bond with the nearest nitrogen from the azo bond. This almost blocked structure make the benzene aromatic protons $H_{3'}$-$H_{6'}$ highly affected by the resonance cone of both double bonds, thus resulting in their consistent resonances shift to higher frequencies (δ^+).

On the other side in the MR-GPTMS derivative (left side of Figure 3), this hydrogen bond can not take place anymore. The optimized structure appears not be planar, but slightly tilted with a dihedral angle for N-N-C1'-C6' of *ca* 16.89 degrees. For this reasoning the two $H_{3'}$ and $H_{6'}$ ortho-protons now lie in the shielding regions (δ^-) of the anisotropic resonance cones of the carbonyl and diazo double bonds, and moves at the lower chemical shifts of 7.54 and 7.51 ppm, respectively.

Figure 3

It has also to be remarked that in the sol MR-GPTMS, the $H_{3'}$ and $H_{6'}$ protons appear as *dd* signals (i.e. doublets of doublets), due to the anomalous low vicinal proton-proton coupling constants ($^3J_{HH}$=5.7 Hz) between the pair of benzene protons $H_{3'}$-$H_{4'}$ and $H_{6'}$-$H_{5'}$ (especially if compared with the value of 7.9 Hz observed in the starting MR), and to the detection of measureable long range coupling constants ($^4J_{HH}$=3.5 Hz).

This $^3J_{HH}$ decrease is due to two concurring effects: (i) increase of the electronegativity of vicinal groups; (ii) longer bond length (i.e. less π-bond order). In the MR-GPTMS derivative the lack of hydrogen bond between the carbonyl and nitrogen of the adjacent azo group, producing a six-ring electron delocalization, make the carboxylic and the diazo fragments more electron withdrawing substituents of the benzene ring, thus affecting particularly the closest $C_{3'}$ and $C_{6'}$, and their corresponding bonded $H_{3'}$ and $H_{6'}$ hydrogens.

In general in aromatic compounds in which π-electrons are delocalized, it has already been observed that vicinal coupling constants decrease with the increasing of bond length, or with the decreasing of π-bond order [33]. In the MR dyes case, the difference between the three bonds coupling constants ($^3J_{HH}$=5.7 Hz for MR-GPTMS *vs* 7.9 Hz for MR) indicates that the corresponding $C_{3'}$–$C_{4'}$ and $C_{5'}$–$C_{6'}$ bond lengths are longer in MR-GPTMS than those in the corresponding starting MR. This behavior can be also explained with the partial localization of the π-electrons of the benzene ring, that makes the $C_{3'}$–$C_{4'}$ and $C_{5'}$–$C_{6'}$ bonds with a more "single" character, than those in MR (see preferred resonance structure for MR and MR-GPTMS shown in Figure 4).

Figure 4

3.3. Photostability and kinetic studies

To study the effect of pH on the decolorization efficiency of the pure MR and MR-GPTMS dyestuffs in aqueous solutions, experiments were carried out at two pH values (2 and 8) using constant dye concentrations, under UV and Visible light irradiations. Figure 5 shows the UV-visible spectra of both MR and MR-GPTMS solutions at acidic and alkaline conditions in different exposure times, under UV source.

When the cleavage of the -N=N- diazo bond occurs, the intensity of the absorbance peak of the solutions decreases. Also, the absorption band shifts slightly from the visible to the UV or IR region of the electromagnetic spectrum, which means that the dye is degraded into lighter compounds. The same photodegradations under visible light were not examined because of the exceedingly slow rate of decolorization. Generally speaking, the color bleaching of dye aqueous solution is a complex process involving many reactions that are difficult to differentiate individually. In fact, a photo-excited dye molecule has a number of photophysical and photochemical degradation pathways which can be followed. Dye degradation can depend on the dye molecule structure, the spectral characteristics of radiation, the composition and structure of the environment and the presence of impurities, such as molecular O_2. In the present study, the experiments were carried out in aerobic condition, where the reaction mixture was always kept in contact with molecular oxygen.

Figure 5

The dissolved oxygen has a tendency to work as an electron sink and thus it participates in the formation of Reactive Oxygen Species (ROS), such as superoxide anions, hydrogen peroxides, and hydroxyl radicals. Nevertheless, in the investigation of the influence of sol-gel based functionalization, preliminary tests have shown that the MR-GPTMS dye has a greater photostability under aerobic conditions than the pure MR. With this reasoning, in the study of the

fading of the two dyestuffs, only the presence of oxygen was assumed as active kinetic species involved in the dye photodegradation process.

Spectrophotometric kinetic studies were undertaken to observe the factors affecting the rate of decolorization. This study was carried out on aqueous solutions of pure MR and MR-GPTMS sol. The dependence of dye concentration on irradiation time was determined by measuring visible absorbance values (λ= 431 nm and 456 nm for MR and MR-GPTMS, respectively, at pH=8; λ= 523 nm for both dyestuffs, at pH= 2) at various irradiation times until 2000 minutes. This method was used to determine the rate constants associated with photodegradation. The absorption spectra were registered at a regular interval time and the absorbance data at a fixed wavelength were fitted as a function of time as a first order kinetic, according to literature [34,35]. Generally first-order kinetics is appropriate for the entire concentration range up to few ppm and several studies were reasonably well fitted by this kinetic model [36].

Based on an established mechanism for the photodegradation of the dyestuff, [37] the rate of photodegradation can be defined by eq. 3:

$$-\frac{dC}{dt} = k[\text{Dye}][O_2] \qquad (3)$$

where C=[*Dye*]$_t$ is the concentration of dye at time t, k is the second-order rate constant ($s^{-1}M^{-1}$) and dC/dt is the rate of change of the dye concentration, respectively.

Since the concentration of O_2 in the air-saturated solution is constant ([O_2]= $3 \cdot 10^{-4}$ M) and is in large excess respect to the dye concentration [37], i.e. [O_2]>>[*Dye*]$_t$, if the initial concentration of dye at time t = 0 is C_0 and at some later time t, the concentration has fallen to C_t, then the integration of equation (3), for t between 0 and t gives eq. 4:

$$-\ln\frac{C_t}{C_0} = k_{obs}\, t \qquad (4)$$

where k_{obs}=k[O_2] is the observed pseudo first-order rate constant (s^{-1}) for the photodegradation process. If we consider the recorded absorbance at different time as Abs_t=ε l C_t (ε=molar absorptivity, l=optical cell path), we can place Abs_t/Abs_0=C_t/C_0. The plot of the - lnC_t/C_0 data *versus*

the irradiation times (t/m) gives straight lines, showing a linear relationship. All reaction traces obeyed a first-order rate law, and pseudo-first-order rate constants for the oxidative photodegradation, k_{obs}/s^{-1}, were obtained from a linear least squares fit of the experimental data to eq.4, with k_{obs} as the parameters to be optimized. These experimental results mean that the photodegradation kinetic of pure and functionalized dyestuffs follow a pseudo-first order rate constant model. The collected results of the fit from the data plotted in Figure 6, i.e. the rates of bleaching of the dyestuffs in water under an UV source irradiation, are reported in Table 1.

Figure 6

Moreover, the results indicated that the pure MR photolytic dyestuff degradation appeared to be the fastest at acidic conditions, since the sol-gel based functionalization decreases dramatically the rate of bleaching of MR-GPTMS dye. In acidic conditions the photodegradation rate of untreated dyestuff is one order of magnitude higher than sol-gel based Methyl Red.

Table 1

At pH 8 the photodegradation rate of MR-GPTMS is six times higher than the pure MR dyestuff. The contribution to the decomposition rate of Methyl Red by photolysis is clearly assigned to pH value and to the presence of GPTMS covalently bonded to carboxyl group of MR.

The observed phenomena of photodegradation mainly involve the breaking of the azo bonds because, as reported in literature [38,39], some radicals are generated *in situ* from the solvent and attack the dye breaking the conjugated π-system and giving rise to decolorisation. By following this mechanism [40,41], OH• radicals can react with most organic compounds by hydrogen abstraction or by addition to double bonds. Thus, in case of MR, OH• radicals first attack azo groups and induces cleavage of the N=N bond, destructing the long conjugated systems and consequently

causing decolorization, owing to the fact that N=N bonds are easier to be destructed than aromatic ring moiety. Consequently, some significant effect on the photodegradation rate should be exerted by the substituents in the diazo system that are able to change the electron density in the region of the diazo group.

It has been shown that sulfonated azo dyes were reduced faster than carboxylated analogues, due to the higher electronegativity of the sulfonyl group, which makes the azo group more accessible to electrons [42]. Likewise, Martins et al. [43] reported that dyes with low polarity and having an electron-donating methyl substituent group in the ring are quite recalcitrant to the photodecomposition. These are in good agreement with the MR capability to form a conformer with an intra-molecular hydrogen bonding, which causes the geometry planar, otherwise twist. As reported in Figure 7, among the six possible conformers of pure Methyl Red dyestuff, only (1) or (4) could form intra-molecular hydrogen bonds between the carboxyl proton and an azo nitrogen atom.

Figure 7

According to literature [44], the (1) geometry has been optimized to be planar while the others twist of ca 30º from the conjugated plane. In the case of conformer (4), the hydrogen bonding is obviously weaker than conformer (1), because it could form a more strained seven-member ring structure *via* hydrogen bonding as seen. The molecular planarity, the energetics or an extension of the N=N azo bond due to an internal hydrogen bonding confirms that molecular π-electrons are delocalized favorably across the whole molecular system [43].

The presence of an ortho-COOH group with respect to the diazo bond could increase the susceptibility of MR to undergo the attack by hydroxyl radicals due to positive electronic effects. Moreover, the proximity between the –COOH and the nitrogen of the diazo bond, may reduce the N=N π overlap, in turn benefiting the dye reactivity toward hydroxyl radicals. The influence of the

position of the carboxyl substitution on the distance of N=N bond, as function of pH on the chemical structure of conformers, has been evaluated in the study of Park et al. [44]. The carboxyl substituent orientation has been determined on conformers (1) and (4) for *o*-MR, under protonated, neutral and anionic conditions, by ab-initio calculations. The measured -N=N- bond length appeared to be shorter in the deprotonated form than in those obtained in acidic or neutral media (1.289 and 1.273 Å for 1 and 4, respectively) [44]. As clearly appear from the kinetic data reported in Table 1, the anionic form of *o*-MR results more stable under UV photodegradation. This is in according to the possibility for the hydrogen of the carboxylic group in the ortho position, to form a hydrogen bond with the nitrogen from the azo bond, thus reducing the electron density around it. The reduced electron density around the azo bond could make it more susceptible to cleavage.

All experimental results led us to conclude that a significant improvement in photostability has been found with Methyl Red dyes functionalized with GPTMS. As a matter of fact, in this latter case a significant influence on the photostability of the dyestuff is exerted by the ester covalent bond between the 3-glycidoxypropyltrimethoxysilane and the carboxyl group in ortho position to the azo bond, if compared to the corresponding non-silylated MR dye. In particular the improved photostability of the sol-gel based dyestuff can be attributed to the new bonds arrangement after the epoxy ring opening reaction by the MR carboxyl group that cannot form anymore an hydrogen bond with the -N=N- group, as also shown by NMR spectroscopy, and consequently, reduce electron density around it. The disappearance of the hydrogen bond allows the increase of the electron density around the azo bond, making it less susceptible to cleavage, and consequently causing an increase in the photostability.

3.4. FT-IR characterization of bleaching MR and MR-GPTMS

Photobleaching products of pure MR and MR-GPTMS dyestuffs after UV irradiation were studied to confirm the degradation of molecules. Figure 8 shows the FTIR spectra of control MR, MR-GPTMS and the extracts from the irradiated samples.

Figure 8

Pure and silylated dyes show characteristic -N=N- asymmetric stretching bond typical of azo dye at 1602 cm^{-1}. Moreover peaks at 2920 cm^{-1} (asymmetric CH_3 stretching vibrations), at 1550-1465 cm^{-1} (C=C–H in plane C–H bend), at 817 cm^{-1} (C-H stretching of p-substituted ring) and a peak at 763 cm^{-1} (C-H stretching of o-substituted ring) are detected in the pure MR spectrum [45].

After irradiations under an UV source, most of bands of pure methyl red, e.g., characteristic band of C–H stretching of aromatic ring at 817 and 763 cm^{-1}, significantly decreased in the spectrum of the extracts. The band at 2920 cm^{-1} is covered by the new broad band in the range 3400-3100 cm^{-1} due to the new formed NH_2 groups after MR decomposition. At the same time, the infrared spectra of the degradation products formed by photolysis had displayed entirely new peaks compared to the initial control dye, which confirms the degradation of MR.

In the spectra of MR-GPTMS, strong Si–O–Si bands at ∼1200 cm^{-1} and ∼1100 cm^{-1} were observed in the FTIR spectra of the start and decomposed product. Characteristic bands of epoxide ring were not observed, in accordance with the results reported by Guido et al. [25], due to the covalent reaction between GPTMS and MR dye. The band at 1602 cm^{-1} and 1713 cm^{-1} are attributed respectively to N=N and C=O stretching of MR. No significant differences were observed in characteristic infrared spectra of GPTMS, before and after UV irradiation, which suggests that the silane is still present also in the decomposition products. While, for MR covalently bonded dye was observed the disappearance of the band at 1602 cm^{-1}, and the shift of the broad band in the range 3400-3100 cm^{-1}, because of the appearance of the NH_2 groups.

Based on these results a degradation pathway was developed for the decolorization of both MR and MR dyestuffs (Scheme 3), in agreement with previous study of the cleavage of the -N=N- diazo bond [46]. We believe that dye degradation begins with the radicals rupture of the N–C(Ar) bond of the azo N=N–Ar moiety to produce the remaining products as shown in Scheme 3.

Scheme 3

The decolorized sols of both MR and MR-GPTMS, as obtained after UV irradiation, have been examined by NMR spectroscopy. The recorded mono and bi-dimensional NMR spectra clearly show the complete occurred disappearance of the proton signals relative to the starting MR and MR-GPTMS dyes, while the expected resonance pattern of newly formed aromatic species, as showed in Scheme 3, is present.

4. Conclusion

The aim of this study was the investigation of MR and MR-GPTMS light stability under both UV and visible irradiation. The photostability behavior were examined in detail, varying the pH. Under UV source, the functionalized Methyl Red has shown an increased photostability at acidic conditions, due to disappeared influence of hydrogen bond onto the -N=N- system than its unfunctionalized counterpart. The study confirmed that the light fastness of the dyestuffs depends on the electron density in the –N=N- reaction center. Nevertheless hydrogen bonding, in addition to the electron density in the region of the azo bond, has a significant effect on the rate of reduction. The substitution of hydroxyl group in the ortho position of the phenyl ring, relative to the azo bond, causes an increase in the photostability of functionalized dyestuff. The silica attached to the dyes, reducing the influence of hydroxyl group on the diazo system, shields the molecules from the photodecomposition under UV radiations, thus enabling the use of such hybrid dyestuffs as lightfast and more efficient halochromic sensors.

Acknowledgments

The authors thank Professor Giuseppe Bruno (University of Messina, Italy) for the useful discussions and comments.

References

[1] E. Ruiz-Hitzky, M. Darder, P. Aranda, K. Ariga, Advances in Biomimetic and Nanostructured Biohybrid Materials, Adv. Mater. 22 (2010) 323–336. doi:10.1002/adma.200901134.

[2] J. Alongi, C. Colleoni, G. Rosace, G. Malucelli, Thermal and fire stability of cotton fabrics coated with hybrid phosphorus-doped silica films, J. Therm. Anal. Calorim. 110 (2012) 1207–1216. doi:10.1007/s10973-011-2142-0.

[3] J.W. Gilliland, K. Yokoyama, W.T. Yip, Solvent effect on mobility and photostability of organic dyes embedded inside silica sol-gel thin films, Chem. Mater. 17 (2005) 6702–6712. doi:10.1021/cm050658h.

[4] D. Avnir, D. Levy, R. Reisfeld, The nature of the silica cage as reflected by spectral changes and enhanced photostability of trapped Rhodamine 6G, J. Phys. Chem. 88 (1984) 5956–5959. doi:10.1021/j150668a042.

[5] A. Makishima, T. Tani, Preparation of Amorphous Silicas Doped with Organic Molecules by the Sol-Gel Process, J. Am. Ceram. Soc. 69 (1986) C–72–C–74. doi:10.1111/j.1151-2916.1986.tb04755.x.

[6] V.R. Kaufman, D. Avnir, D. Pines-Rojanski, D. Huppert, Water consumption during the early stages of the sol-gel tetramethylorthosilicate polymerization as probed by excited state proton transfer, J. Non. Cryst. Solids. 99 (1988) 379–386. doi:10.1016/0022-3093(88)90443-7.

[7] J. Pouxviel, B. Dunn, J. Zink, Fluorescence study of aluminosilicate sols and gels doped with hydroxy trisulfonated pyrene, J. Phys. Chem. 93 (1989) 2134–2139. doi:10.1021/j100342a082.

[8] J. Fitremann, S. Doeuff, C. Sanchez, Propriétés Optiques de Gels à Base de TiO2, ZrO2, Al2O3 et SiO2 Dopés par de la Rhodamine 640, Ann. Chim. Des Mater. 15 (1990) 421–432.

[9] D. Levy, F. Del Monte, J.M. Otón, G. Fiksman, I. Matías, P. Datta, et al., Photochromic doped sol-gel materials for fiber-optic devices, J. Sol-Gel Sci. Technol. 8 (1997) 931–935. doi:10.1007/BF02436963.

[10] M.A. García-Sánchez, A. Campero, M.D.L. Avilés C, Decomposition of metal tetrasulphophthalocyanines incorporated in SiO2 gels, J. Non. Cryst. Solids. 351 (2005) 962–969. doi:10.1016/j.jnoncrysol.2004.12.006.

[11] C. Colleoni, E. Guido, V. Migani, G. Rosace, Hydrophobic behaviour of non-fluorinated sol-gel based cotton and polyester fabric coatings, J. Ind. Text. 44 (2015) 815–834. doi:10.1177/1528083713516664.

[12] J. Alongi, C. Colleoni, G. Rosace, G. Malucelli, Phosphorus- and nitrogen-doped silica coatings for enhancing the flame retardancy of cotton: Synergisms or additive effects?, Polym. Degrad. Stab. 98 (2013) 579–589. doi:10.1016/j.polymdegradstab.2012.11.017.

[13] J. Alongi, C. Colleoni, G. Rosace, G. Malucelli, The role of pre-hydrolysis on multi step sol-gel processes for enhancing the flame retardancy of cotton, Cellulose. 20 (2013) 525–535. doi:10.1007/s10570-012-9806-1.

[14] R. Poli, C. Colleoni, A. Calvimontes, H. Polášková, V. Dutschk, G. Rosace, Innovative sol–gel route in neutral hydroalcoholic condition to obtain antibacterial cotton finishing by zinc precursor, J. Sol-Gel Sci. Technol. 74 (2015) 151–160. doi:10.1007/s10971-014-3589-9.

[15] B. Mahltig, T. Textor, Silver containing sol-gel coatings on polyamide fabrics as antimicrobial finish-description of a technical application process for wash permanent antimicrobial effect, Fibers Polym. 11 (2010) 1152–1158. doi:10.1007/s12221-010-1152-z.

[16] C. Colleoni, M.R. Massafra, G. Rosace, Photocatalytic properties and optical characterization of cotton fabric coated via sol‑gel with non‑crystalline TiO2 modified with poly(ethylene glycol), Surf. Coatings Technol. 207 (2012) 79‑88. doi:10.1016/j.surfcoat.2012.06.003.

[17] B. Mahltig, H. Bottcher, D. Knittel, E. Schollmeyer, Light Fading and Wash Fastness of Dyed Nanosol-Coated Textiles, Text. Res. J. 74 (2004) 521–527. doi:10.1177/004051750407400610.

[18] M. Caldara, C. Colleoni, E. Guido, V. Re, G. Rosace, Development of a textile-optoelectronic pH meter based on hybrid xerogel doped with Methyl Red, Sensors Actuators, B Chem. 171-172 (2012) 1013–1021. doi:10.1016/j.snb.2012.06.024.

[19] L. Van Der Schueren, K. De Clerck, G. Brancatelli, G. Rosace, E. Van Damme, W. De Vos, Novel cellulose and polyamide halochromic textile sensors based on the encapsulation of Methyl Red into a sol-gel matrix, Sensors Actuators, B Chem. 162 (2012) 27–34. doi:10.1016/j.snb.2011.11.077.

[20] L. Feng, C.J. Musto, J.W. Kemling, S.H. Lim, W. Zhong, K.S. Suslick, Colorimetric Sensor Array for Determination and Identification of Toxic Industrial Chemicals, Anal. Chem. 82 (2010) 9433–9440. doi:10.1021/ac1020886.

[21] A.D.F. Dunbar, S. Brittle, T.H. Richardson, J. Hutchinson, C.A. Hunter, Detection of volatile organic compounds using porphyrin derivatives, J. Phys. Chem. B. 114 (2010) 11697–11702. doi:10.1021/jp102755h.

[22] M. Plaschke, R. Czolk, H.J. Ache, Fluorimetric determination of mercury with a water-soluble porphyrin and porphyrin-doped sol-gel films, Anal. Chim. Acta. 304 (1995) 107–113. doi:10.1016/0003-2670(94)00568-7.

[23] D.R. Walt, C. Munkholm, P. Yuan, S. Luo, S. Barnard, Chemical Sensors and Microinstrumentation, in: R.W. Murray, R.E. Dessy, W.R. Heineman, J. Janata, W.R. Seitz (Eds.), American Chemical Society, Washington, DC, 1989: pp. i–vi. doi:10.1021/bk-1989-0403.

[24] A. Morales-Bahnik, R. Czolk, J. Reichert, H.J. Ache, An optochemical sensor for Cd(II) and Hg(II) based on a porphyrin immobilized on Nafion® membranes, Sensors Actuators B Chem. 13 (1993) 424–426. doi:10.1016/0925-4005(93)85417-9.

[25] E. Guido, C. Colleoni, K. De Clerck, M.R. Plutino, G. Rosace, Influence of catalyst in the synthesis of a cellulose-based sensor: Kinetic study of 3-glycidoxypropyltrimethoxysilane epoxy ring opening by Lewis acid, Sensors Actuators, B Chem. 203 (2014) 213–222. doi:10.1016/j.snb.2014.06.126.

[26] M. Ucar, A.O. Solak, N. Menek, Electrochemical Behavior of 2'-Halogenated Derivatives of N,N-Dimethyl-4-aminoazobenzene at Mercury Electrode., Anal. Sci. 18 (2002) 997–1002. doi:10.2116/analsci.18.997.

[27] V. Migani, H. Weiss, M.R. Massafra, A. Merlo, C. Colleoni, G. Rosace, Poly-dimethylsiloxane derivates side chains effect on syntan functionalized Polyamide fabric, Appl. Surf. Sci. 257 (2011) 3904–3912. doi:10.1016/j.apsusc.2010.11.117.

[28] Spartan '02, Wavefunction, Inc., Irvine, CA.

[29] J.H. Zhang, Q. Liu, Y.M. Chen, Z.Q. Liu, C.W. Xu, Determination of acid dissociation constant of methyl red by multi-peaks Gaussian fitting method based on UV-visible absorption spectrum, Wuli Huaxue Xuebao/ Acta Phys. - Chim. Sin. 28 (2012) 1030–1036. doi:10.3866/PKU.WHXB201203025.

[30] M. Zhou, Q. Yu, L. Lei, G. Barton, Electro-Fenton method for the removal of methyl red in an efficient electrochemical system, Sep. Purif. Technol. 57 (2007) 380–387. doi:10.1016/j.seppur.2007.04.021.

[31] S. Jurmanović, Š. Kordić, M.D. Steinberg, I.M. Steinberg, Organically modified silicate thin films doped with colourimetric pH indicators methyl red and bromocresol green as pH responsive sol–gel hybrid materials, Thin Solid Films. 518 (2010) 2234–2240. doi:10.1016/j.tsf.2009.07.158.

[32] L. Gabrielli, L. Connell, L. Russo, J. Jiménez-Barbero, F. Nicotra, L. Cipolla, et al., Exploring GPTMS reactivity against simple nucleophiles: chemistry beyond hybrid materials fabrication, RSC Adv. 4 (2014) 1841–1848. doi:10.1039/C3RA44748K.

[33] M. Balci, Basic 1H- and 13C-NMR Spectroscopy, Elsevier, London, 2005.

[34] J. Wu, T. Wang, Ozonation of aqueous azo dye in a semi-batch reactor, Water Res. 35 (2001) 1093–1099. doi:10.1016/S0043-1354(00)00330-4.

[35] M. Neamtu, A. Yediler, I. Siminiceanu, A. Kettrup, Oxidation of commercial reactive azo dye aqueous solutions by the photo-Fenton and Fenton-like processes, J. Photochem. Photobiol. A Chem. 161 (2003) 87–93. doi:10.1016/S1010-6030(03)00270-3.

[36] T. Caronna, C. Colleoni, S. Dotti, F. Fontana, G. Rosace, Decomposition of a phthalocyanine dye in various conditions under UV or visible light irradiation, J. Photochem. Photobiol. A Chem. 184 (2006) 135–140. doi:10.1016/j.jphotochem.2006.04.006.

[37] S. Yang, H. Tian, H. Xiao, X. Shang, X. Gong, S. Yao, et al., Photodegradation of cyanine and merocyanine dyes, Dye. Pigment. 49 (2001) 93–101. doi:10.1016/S0143-7208(01)00012-2.

[38] M.A. Rauf, S.S. Ashraf, Radiation induced degradation of dyes—An overview, J. Hazard. Mater. 166 (2009) 6–16. doi:10.1016/j.jhazmat.2008.11.043.

[39] A.S. Özen, V. Aviyente, R.A. Klein, Modeling the Oxidative Degradation of Azo Dyes: A Density Functional Theory Study, J. Phys. Chem. A. 107 (2003) 4898–4907. doi:10.1021/jp026287z.

[40] M.A. Oturan, J. Pinson, D. Deprez, B. Terlain, Polyhydroxylation of salicylic acid by electrochemIcally generated OH radicals, New J. Chem. 16 (1992) 705–710.

[41] N. Daneshvar, D. Salari, A.R. Khataee, Photocatalytic degradation of azo dye acid red 14 in water: investigation of the effect of operational parameters, J. Photochem. Photobiol. A Chem. 157 (2003) 111–116. doi:10.1016/S1010-6030(03)00015-7.

[42] H.G. Kulla, Biodegradation of synthetic organic colorants, in: T. Leisinger, R. Hutter, A. Cook, J. Nuesch (Eds.), Microb. Degrad. Xenobiotics Recalcitrant Compd. FEMS Symp. No. 12, Academic Press, London, 1981.

[43] M.A.M. Martins, M.H. Cardoso, M.J. Queiroz, M.T. Ramalho, A.M.O. Campus, Biodegradation of azo dyes by the yeast Candida zeylanoides in batch aerated cultures, Chemosphere. 38 (1999) 2455–2460. doi:10.1016/S0045-6535(98)00448-2.

[44] S.-K. Park, C. Lee, K.-C. Min, N.-S. Lee, Structural and Conformational Studies of ortho-, meta-, and para-Methyl Red upon Proton Gain and Loss, Bull. Korean Chem. Soc. 26 (2005) 1170–1176. doi:10.5012/bkcs.2005.26.8.1170.

[45] D.H. Williams, I. Fleming, Spectroscopic Methods In Organic Chemistry, 2nd ed., McGraw-Hill Co. Ltd, 1973.

[46] P.K. Wong, P.Y. Yuen, Decolorization and biodegradation of methyl red by Klebsiella pneumoniae RS-13, Water Res. 30 (1996) 1736–1744. doi:10.1016/0043-1354(96)00067-X.

CAPTIONS

Scheme 1. Synthetic pathway for the formation of the alkoxysilane functionalized MR-GPTMS starting from the MR dye and GPTMS.

Scheme 2. Equilibria schemes taking place on the MR dye upon acid/base addition in aqueous solution, through gradual colour changes from red to yellow (pH=4.2-6.3).

Scheme 3. Proposed pathway for the photodegradation of pure MR dyestuff.

Figure 1. Normalized UV–visible spectra of MR (solid line) and MR-GPTMS sol (dashed line) as a function of pH.

Figure 2. ^{1}H NMR stacked spectra relative to the signal variations for the GPTMS-like moiety and the MR dye in the aliphatic (upper side) in the aromatic region (lower side), respectively, upon formation of the sol-derivative MR-GPTMS (500MHz, T=298K, acetone-d_6).

Figure 3. Conformational structures for MR-GPTMS (left side) and MR (right side) dyes, as obtained by semi-empirical calculation, showing the interaction between the resonance cone of the carbonyl (red circle) and azo (blue circle) double bonds on the shielding (δ+) and deshielding (δ-) of the benzene methine proton signals, respectively.

Figure 4. Dominating resonance structures for MR and MR-GPTMS.

Figure 5. UV-visible spectral changes of MR and MR-GPTMS sol upon UV degradation at pH 2 and 8.

Figure 6. Rate of disappearance of MR and MR- GPTMS, in aqueous solutions at different pH conditions (pH=2 and 8; T=298K).

Figure 7. Lowest energy calculated structures of neutral MR together with their structural representations of the six possible conformations.

Figure 8. IR spectra for Methyl Red (upper spectrum), and MR-GPTMS (lower spectrum). For each dyestuff are reported the related decomposition products.

Table(s)

Table 1. UV photodegradation rates of both MR and MR-GPTMS systems at pH 2 and 8.*

pH	Dye	k_{obs}/s^{-1}	R^2
2	MR	3.83×10^{-5}	0.9965
	MR-GPTMS	3.83×10^{-5}	0.9937
8	MR	1.02×10^{-5}	0.9961
	MR-GPTMS	1.67×10^{-6}	0.9943

* In water as solvent at T=298K. The observed rate constants were each determined on 5 independent kinetic runs.

Figure(s)

Scheme 1.

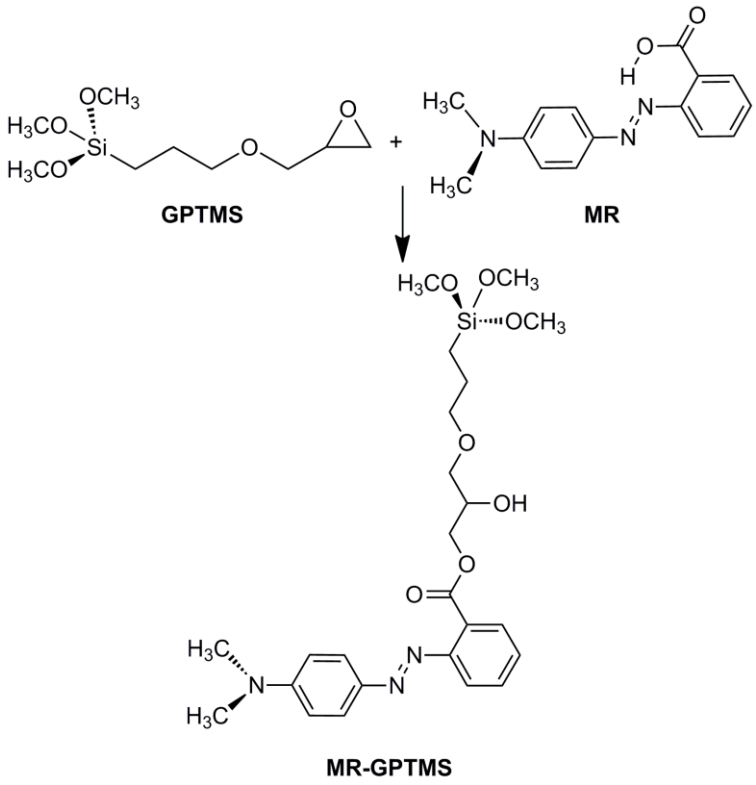

Figure 1

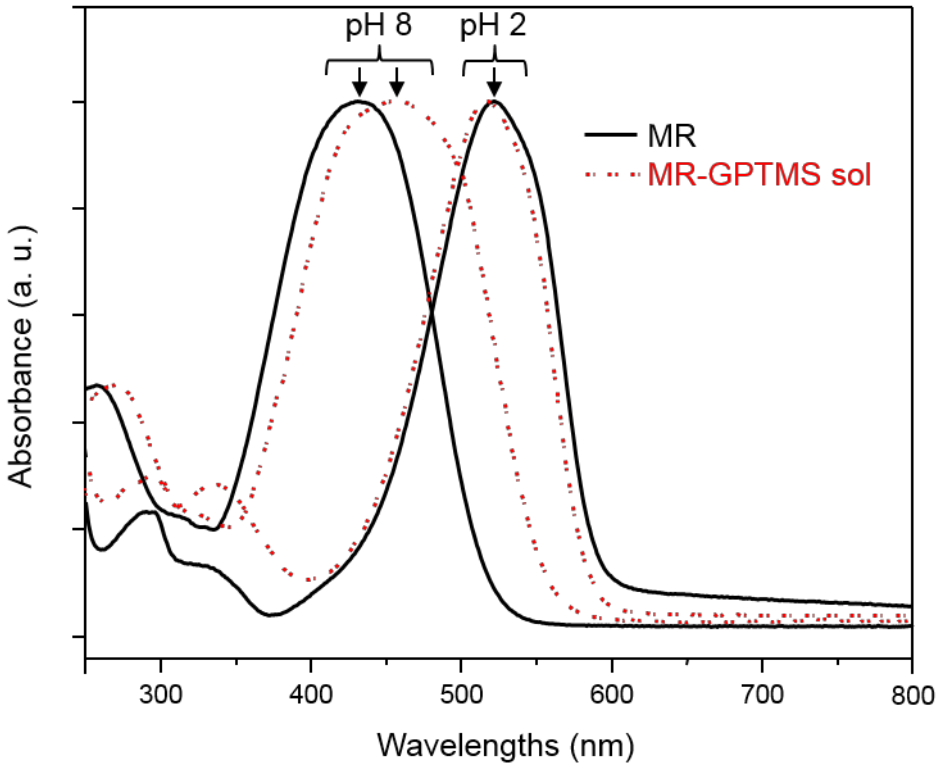
pH 8
pH 2
MR
MR-GPTMS sol
Absorbance (a. u.)
300
400
500
600
700
800
Wavelengths (nm)

Scheme 2

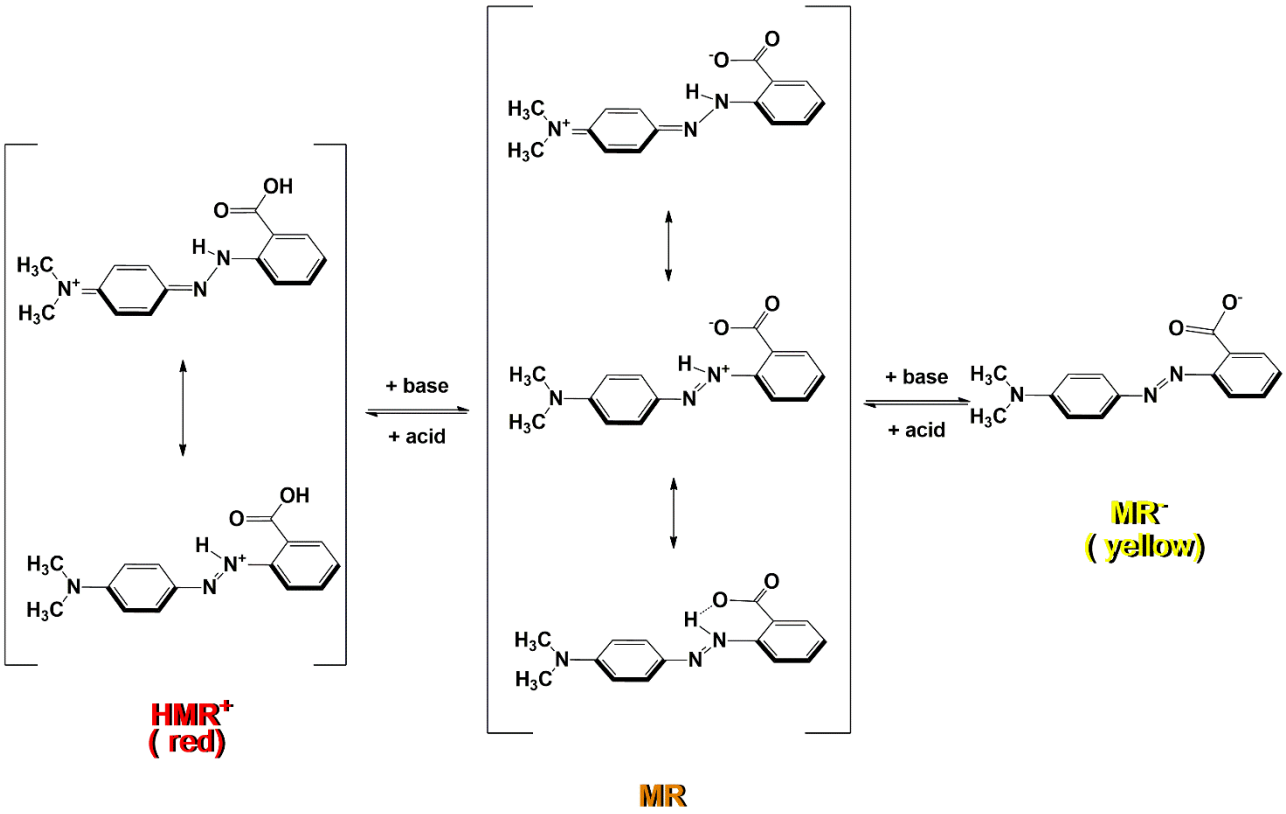

Figure 2

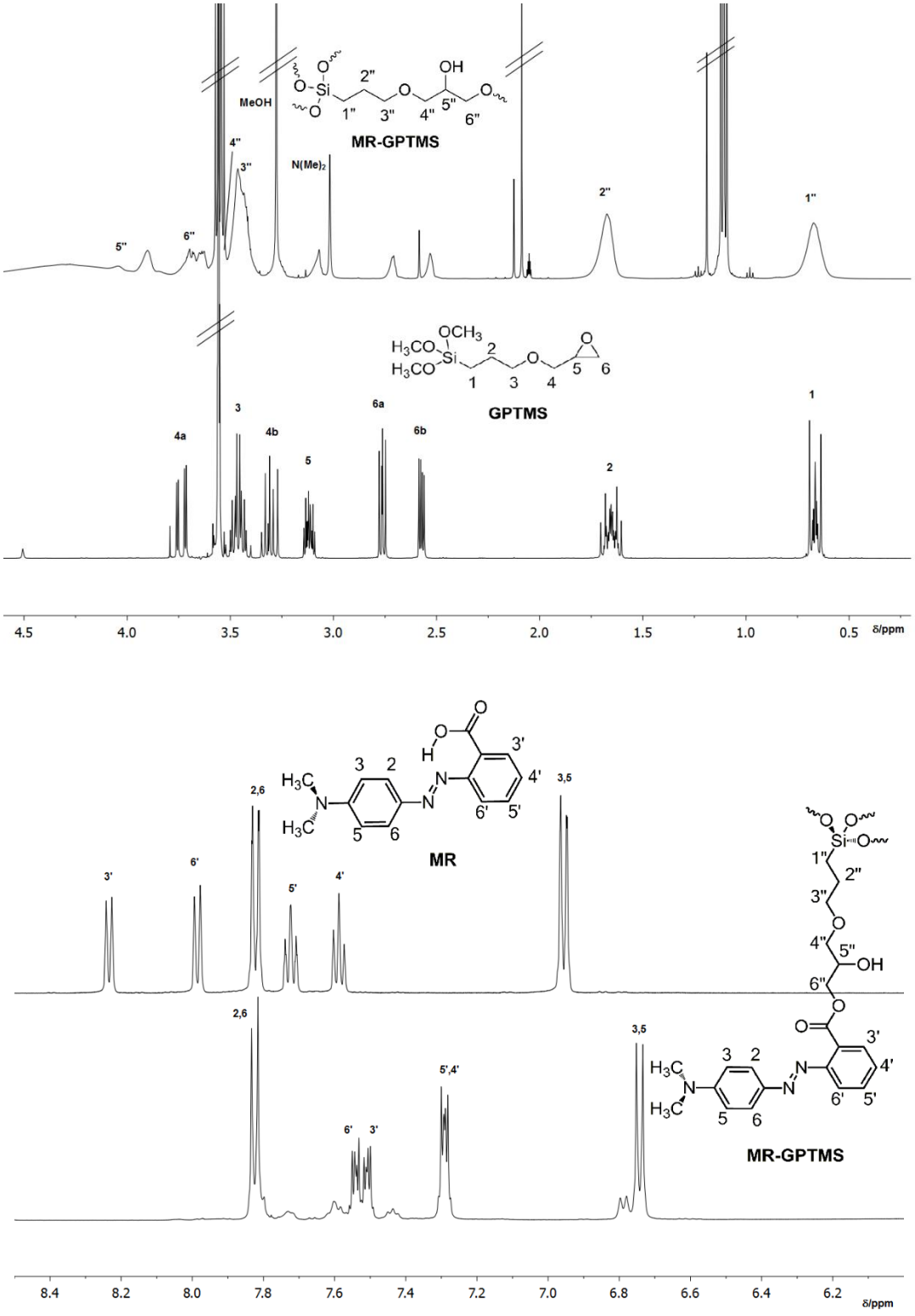

Figure 3

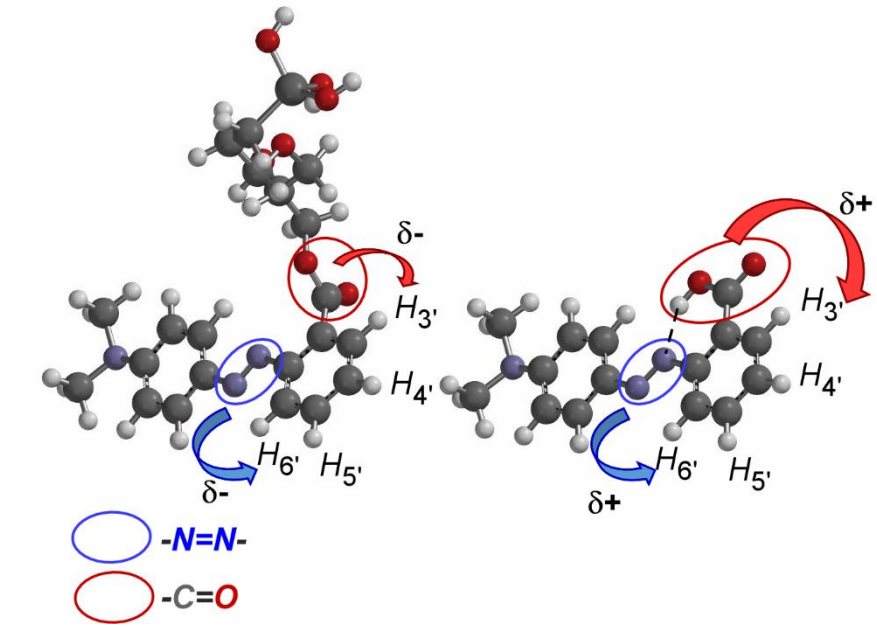

Figure 4

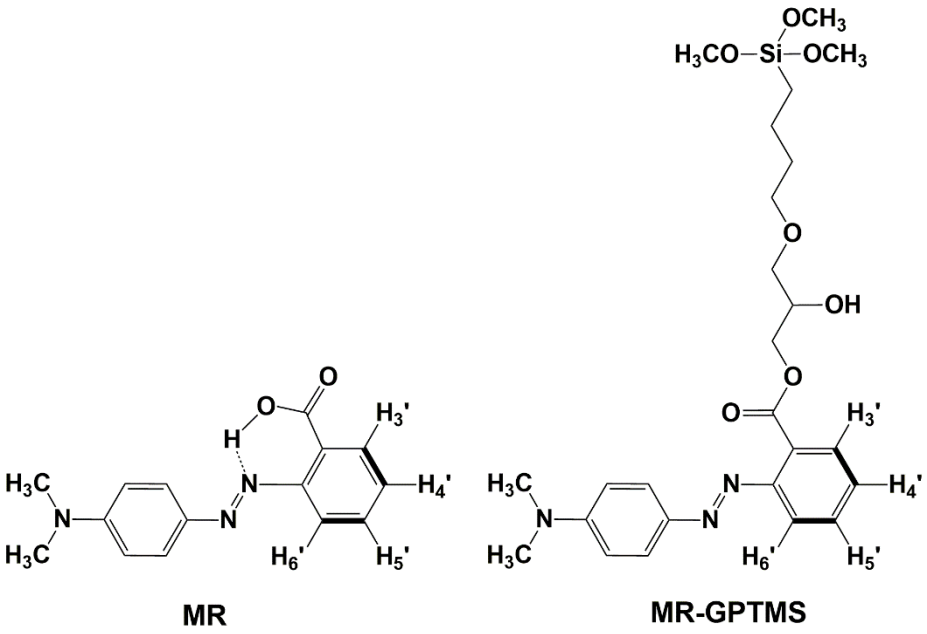

Figure 5

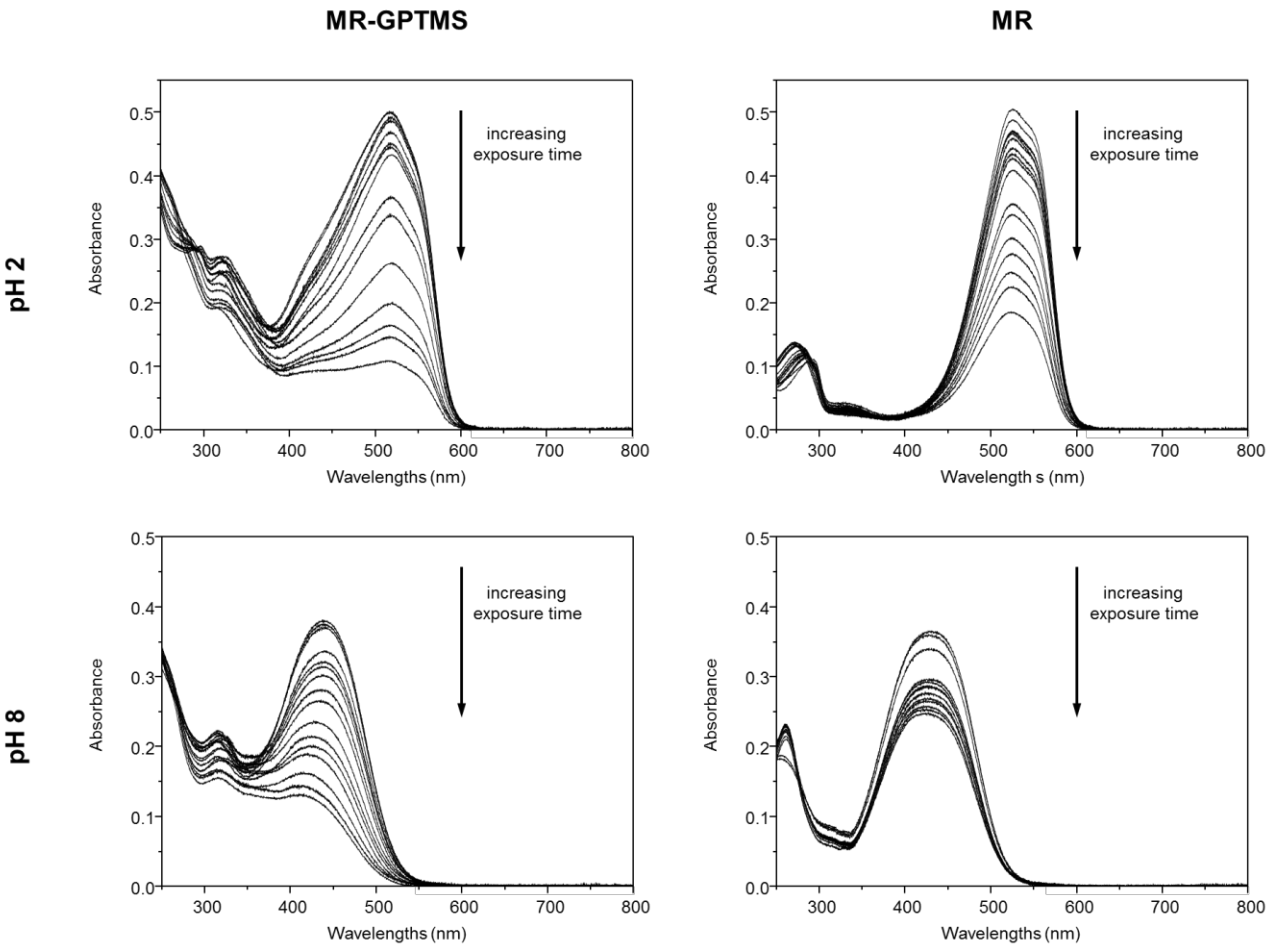
MR-GPTMS
MR
pH 2
pH 8
increasing exposure time
Absorbance
Wavelengths (nm)
Wavelength s (nm)
0.0
0.1
0.2
0.3
0.4
0.5
300
400
500
600
700
800

Figure 6

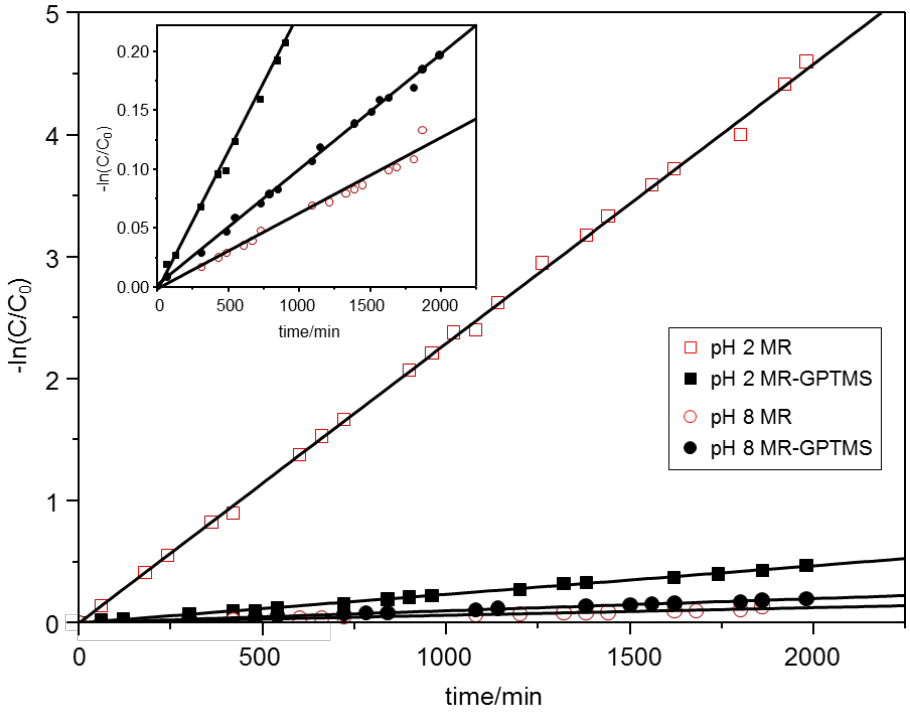
-ln(C/C0)
time/min
pH 2 MR
pH 2 MR-GPTMS
pH 8 MR
pH 8 MR-GPTMS
-ln(C/C0)
time/min

Figure 7

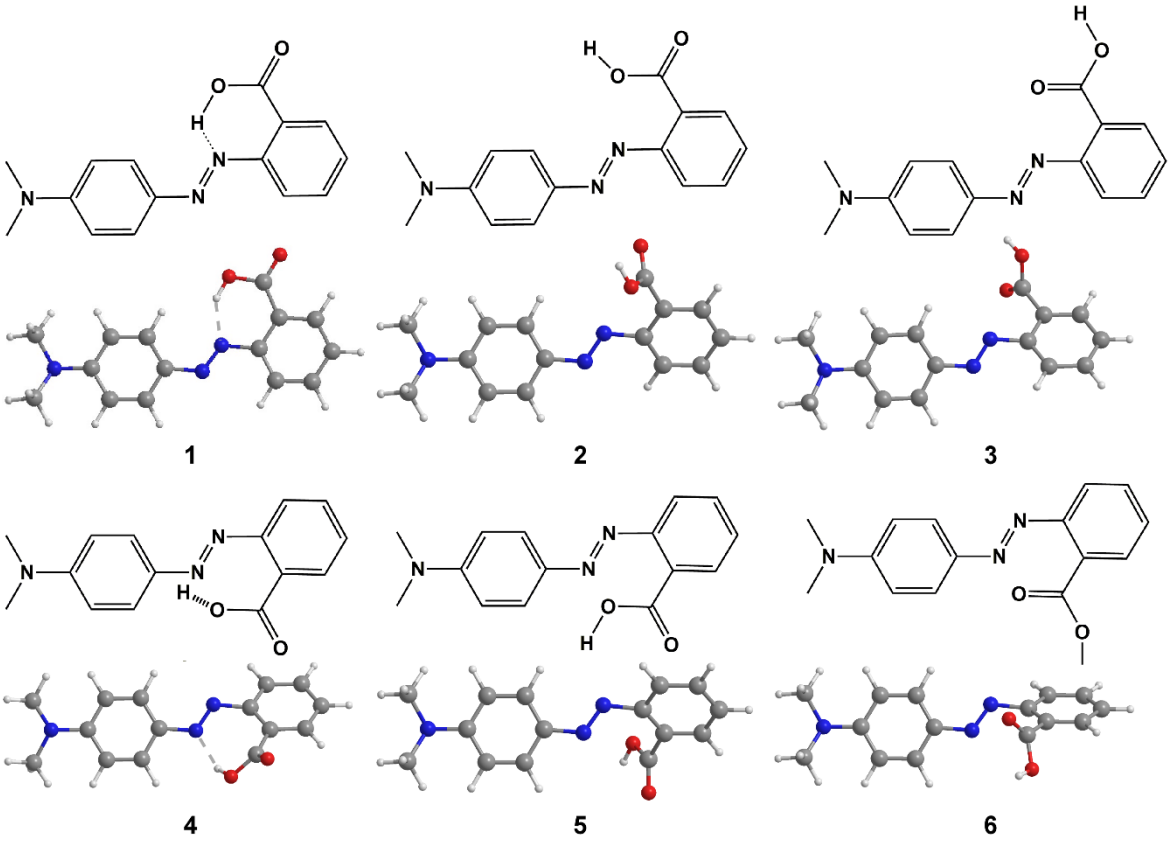

Figure 8

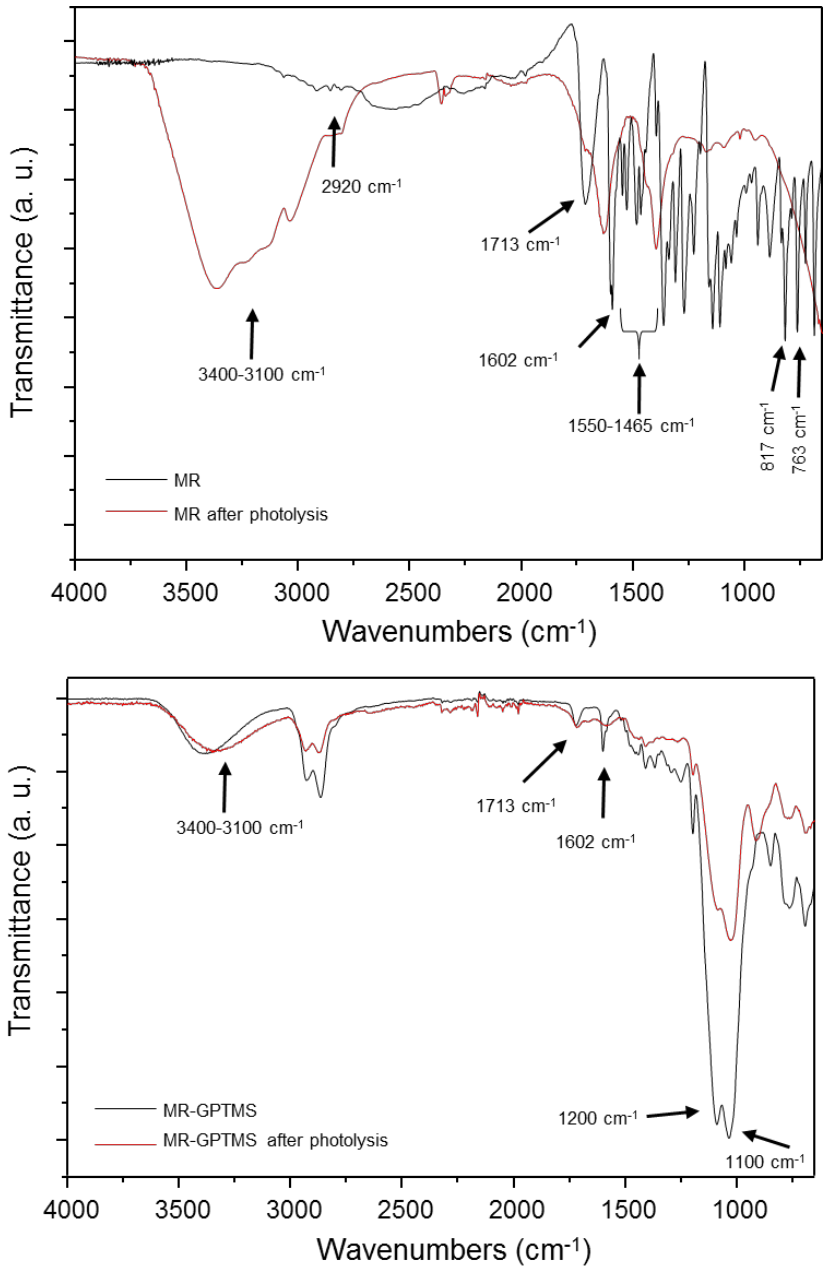
Transmittance (a. u.)
2920 cm-1
1713 cm-1
3400-3100 cm-1
1602 cm-1
1550-1465 cm-1
817 cm-1
763 cm-1
MR
MR after photolysis
4000
3500
3000
2500
2000
1500
1000
Wavenumbers (cm-1)
Transmittance (a. u.)
3400-3100 cm-1
1713 cm-1
1602 cm-1
MR-GPTMS
MR-GPTMS after photolysis
1200 cm-1
1100 cm-1
4000
3500
3000
2500
2000
1500
1000
Wavenumbers (cm-1)

Scheme 3

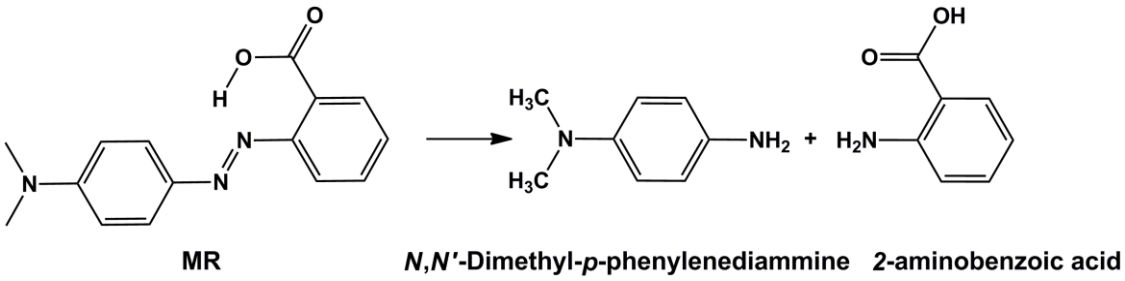

MR *N*,*N*′-Dimethyl-*p*-phenylenediammine *2*-aminobenzoic acid

Authors Biographies

Maria Rosaria Plutino obtained her Ph.D. in Chemistry Science in 1997 at University of Messina, Italy. In 1999 she was appointed temporary researcher at the Institute of Chemistry and Technology of natural Products (ICTPN) – CNR, Unity of Messina. Since December 2001 she is a researcher at the Institute for the Study of Nanostructured Materials, in Messina, Italy. Her research activity is mainly focused on the synthesis, the structural study and characterization of supramolecular nano- and mesostructured assemblies, obtained by spontaneous organization of transition metal complexes and polyfunctionalized organic ligands, in solution or supported on organic/inorganic solid matrix.

Emanuela Guido graduated in Chemistry at the University of Messina (Italy) in 2006. Her doctoral research in organometallic synthesis was started in 2007 at the same institution, from which she received the Ph.D. degree in 2010. Between 2010 and 2011 she held a post-doctoral position at the University of Messina (Italy) for the study and development of organometallic compounds for cancer therapy. Currently she works at the University of Bergamo (Italy) where her research interests deal with the study and development of hybrid organic–inorganic materials for functional textiles.

Claudio Colleoni received his master of Engineering in 2007 at Bergamo University (Italy). In 2012, he obtained his Ph.D. on the deposition of hybrid organic–inorganic materials for functional textiles. Since April 2012 he is holding a post-doctoral position at the University of Bergamo (Italy). His research activities are focused on colloidal chemistry and nanotechnology for sensor material, enzymes immobilization and textile surface functionalization.

Giuseppe Rosace obtained his Ph.D. in Chemistry Science in 1995 at University of Messina (Italy). During the period 2001-2004 he held a lecture position of "Textile finishing" at the University of

Bergamo, where since 2005 he was appointed as an Assistant Professor. His research activities are mainly focused on colloidal chemistry and on synthesis and characterization of organic-inorganic hybrid for functionalization of polymer surfaces. He is author or coauthor of more than 100 papers on international scientific journals and conference proceedings.